

## Supporting Information

### **Zr vacancy interface: an effective strategy for collaborative optimization of ZrNiSn-Based thermoelectric performance**

Yihua Zhang,<sup>‡a</sup> Shuankui Li,<sup>‡b</sup> Fusheng Liu,<sup>\*a</sup> Chaohua Zhang,<sup>a</sup> Lipeng Hu,<sup>a</sup>

Weiqin Ao,<sup>a</sup> Yu Li,<sup>a</sup> Junqing Li,<sup>a</sup> Heping Xie,<sup>a</sup> Yinguo Xiao,<sup>\*b</sup> and Feng Pan<sup>\*b</sup>

<sup>‡</sup> These authors contributed equally to this work

<sup>a</sup>Shenzhen Key Laboratory of Special Functional Materials, Shenzhen Engineering Laboratory for Advanced Technology of Ceramics, Guangdong Research Center for Interfacial Engineering of Functional Materials, College of Materials Science and Engineering, Institute of Deep Underground Sciences and Green Energy, Shenzhen University, Shenzhen 518060, P.R. China

<sup>b</sup>School of Advanced Materials, Peking University Shenzhen Graduate School, Shenzhen, 518055, P.R. China

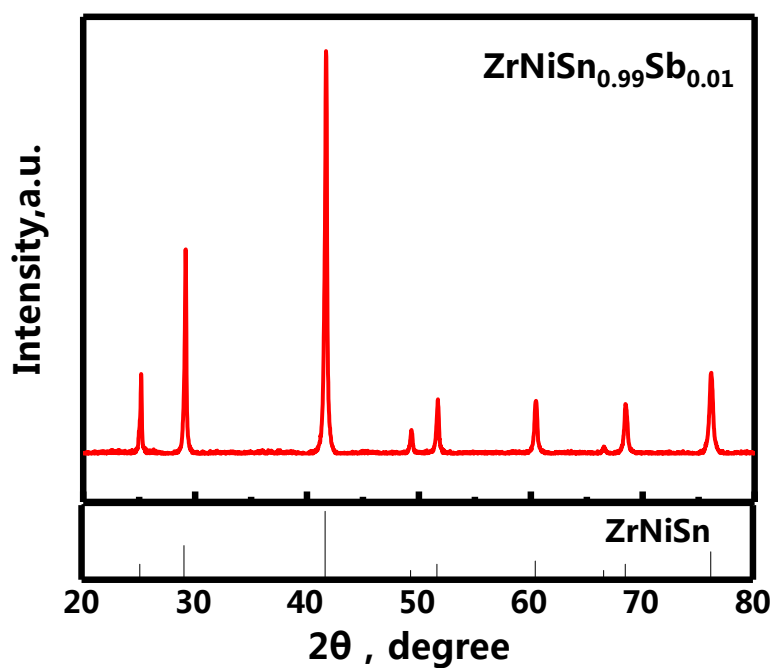


**Fig S1.** XRD pattern of the as-prepared  $\text{ZrNiSn}_{0.99}\text{Sb}_{0.01}$  (ZNSS) powders.

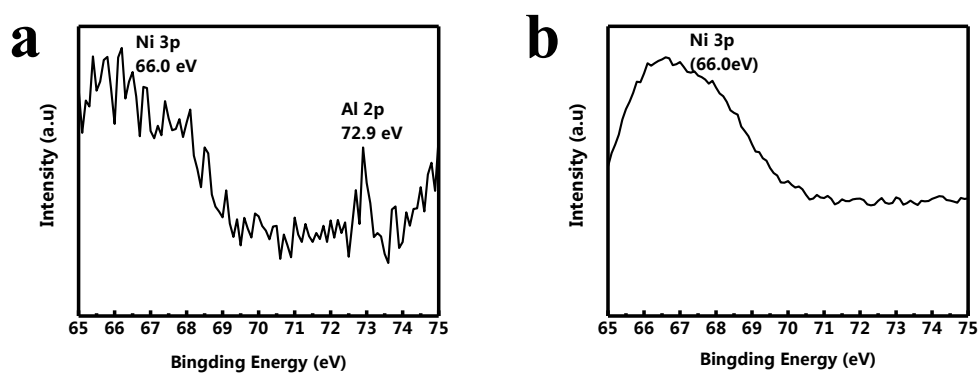


**Fig S2.** (a) XPS spectra for the as-prepared ZNSS with ultra-thin  $\text{Al}_2\text{O}_3$  interface layer and (b) the sintered ALD coated ZNSS sample.

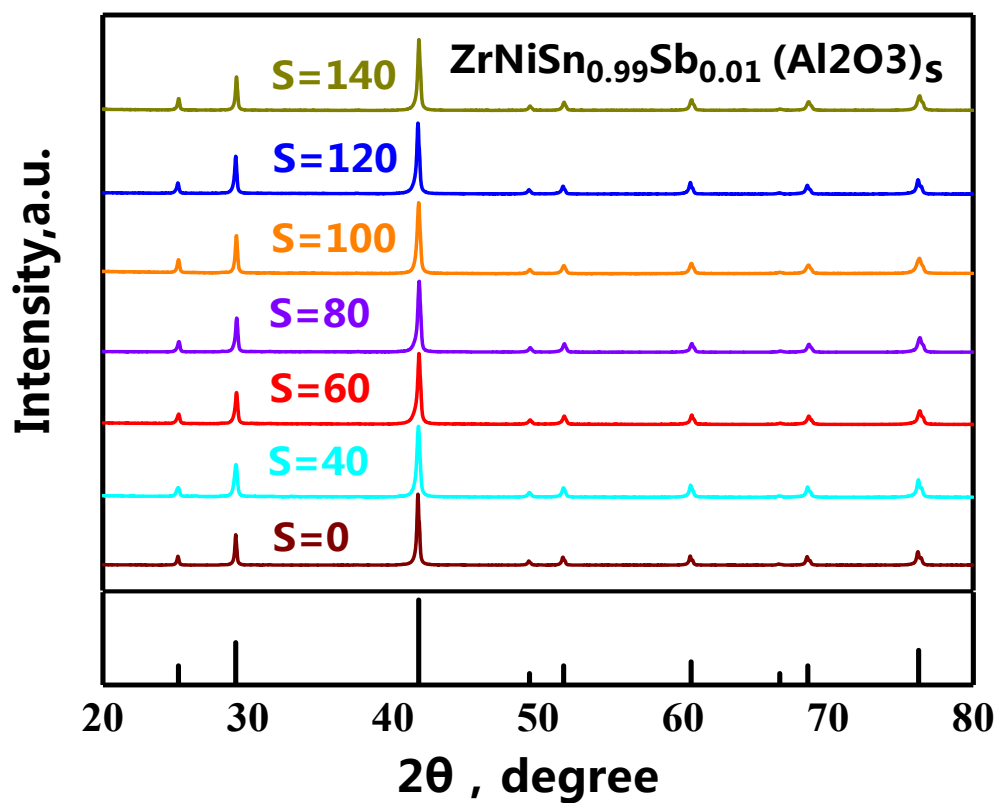
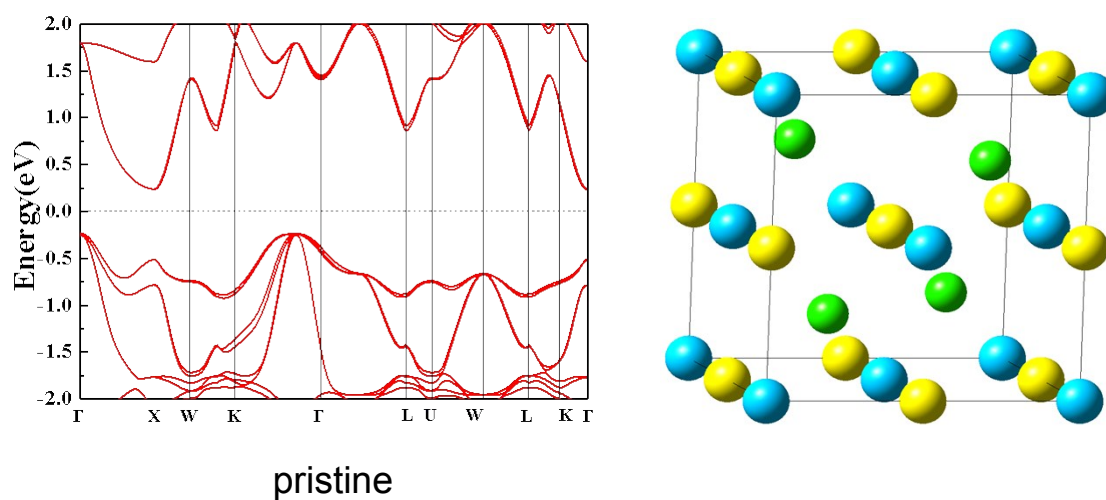
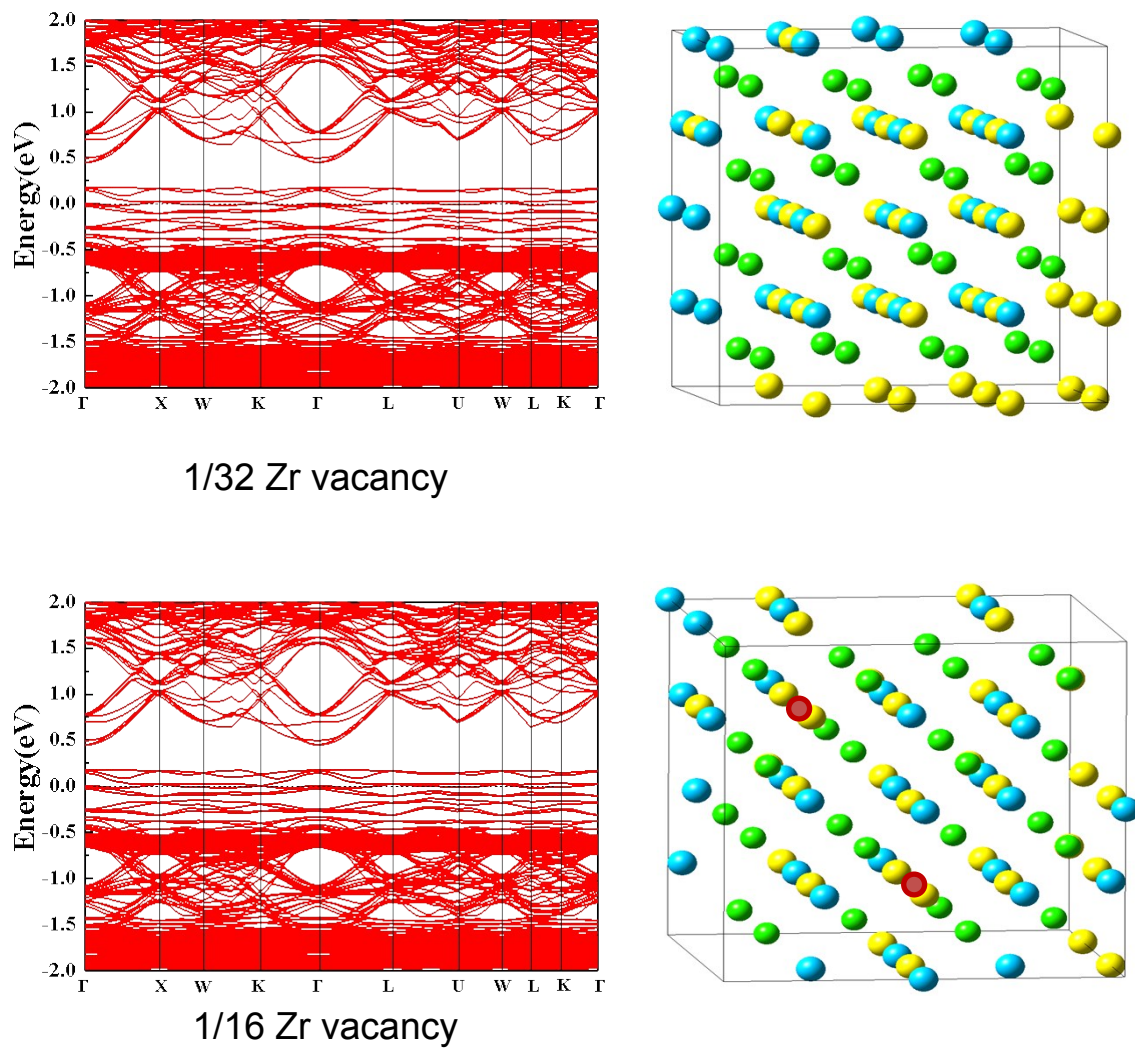


Fig S3. XRD pattern of the samples with different ALD cycles after SPS process.





**Fig S4.** Schematic diagram and band structure diagram of ZrNiSn and different Zr vacancies. The impurity level is located at the position of the blue dotted line in Fig. b and c.

$Zr_{(1-x)}NiSn$	bottom of conduction band	energy barrier
$x=0$	0.236 eV	0 eV
$x=1/32$	0.411 eV	0.175 eV
$x=1/16$	0.447 eV	0.211 eV

**Table S1.** The position of the bottom of conduction band of different Zr vacancies and the interface barrier between energy band of different Zr vacancies and matrix ZNSS

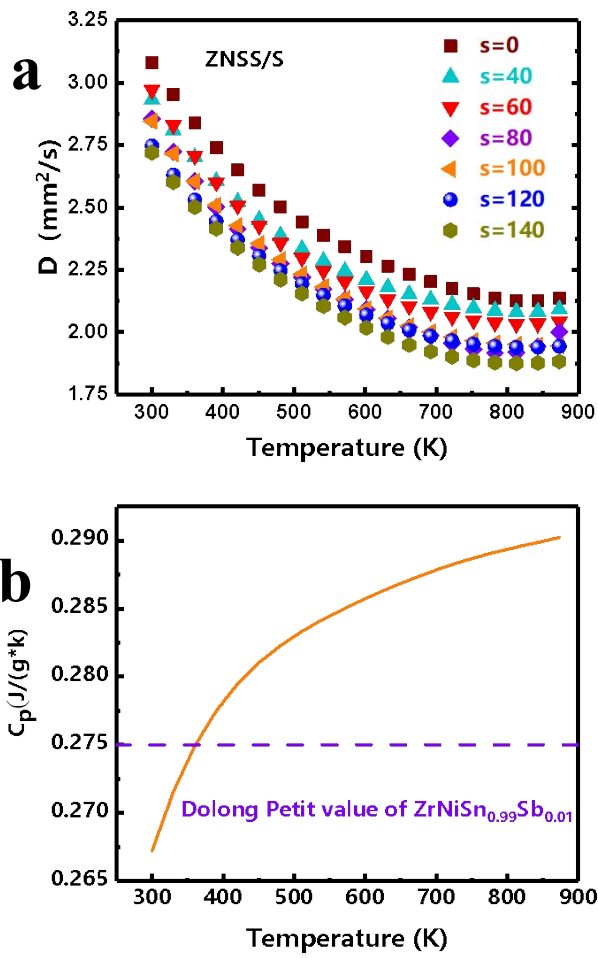


**Fig S5.** (a) Temperature dependence of Thermal diffusion coefficient ( $D$ ) with different ALD cycles. (b) Temperature dependent specific heat capacity  $C_p$  for ZNSS.

These  $m^*$  values were used to plot Pisarenko lines that demonstrate carrier concentration dependence of the Seebeck coefficient in degenerate semiconductors via the following equation:

$$S = \frac{8\pi^2 k_B^2 T}{3eh^2} m_d^* \left( \frac{\pi}{3n} \right)^{2/3} \quad (1)$$

where  $m_d^*$  is the density of states (DOS) effective mass, and  $k_B$ ,  $e$ , and  $h$  are the Boltzmann constant, elementary charge, and the Planck constant, respectively. By utilizing the  $S$  and  $n$  values at room temperature, the  $m_d^*$  was determined and compared with literature data.

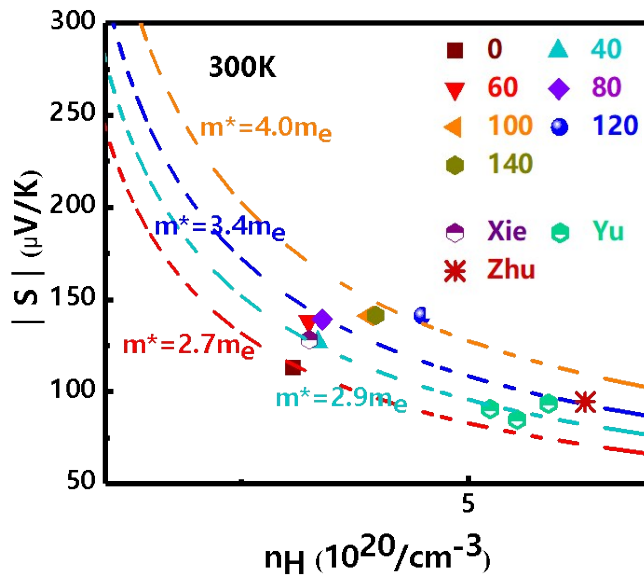
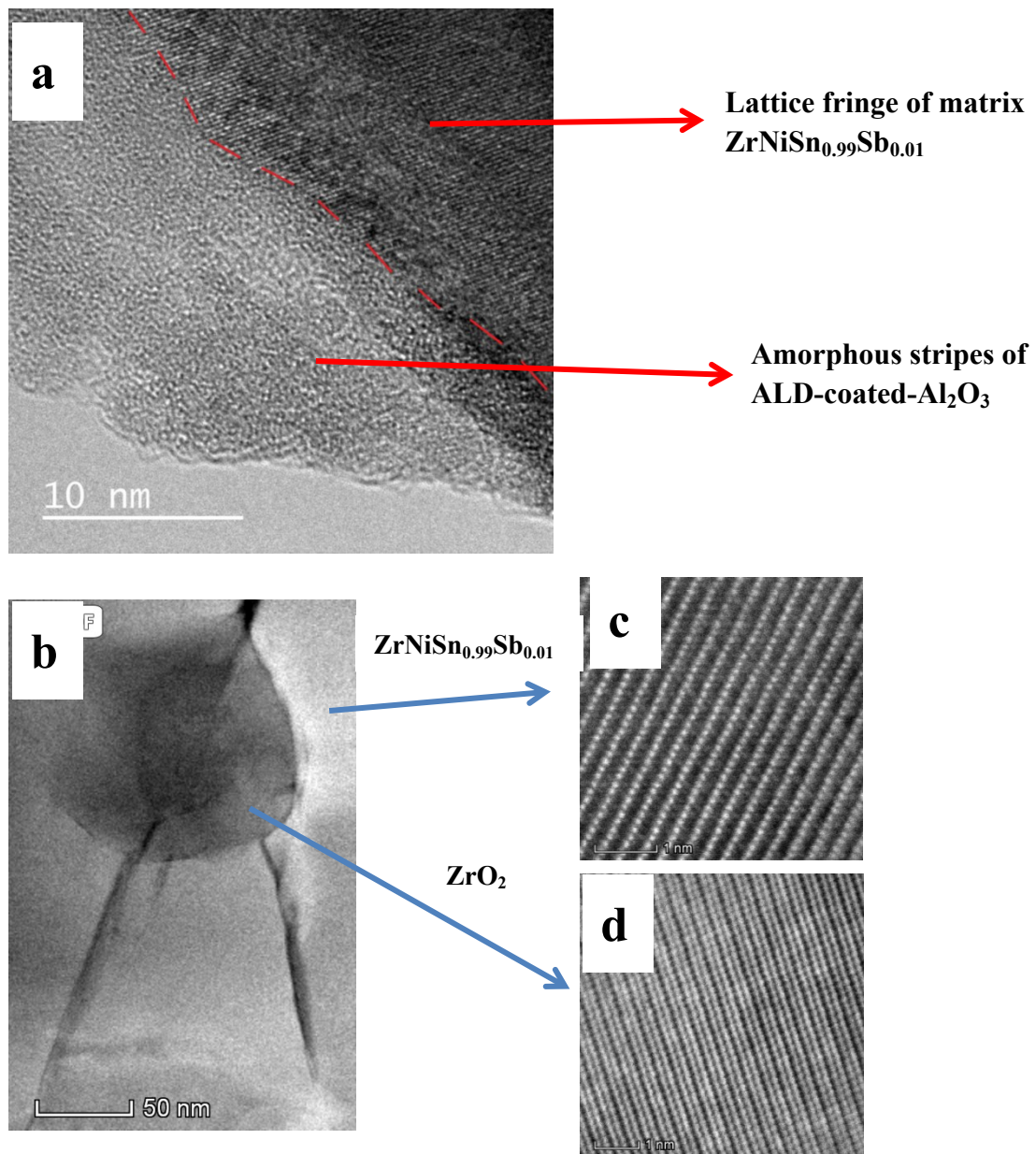


Fig. S6 Carrier-concentration- dependent Seebeck coefficient (S).



**Fig. S7** (a) HRTEM images at the ZnO/BTS interface of pre-sintered powder. (b) Low magnification TEM image, (c) (d) HRTEM images at the  $\text{ZrO}_2/\text{ZNSS}$  interface of sintered sample